Article:
Auer, S orcid.org/0000-0003-0418-1745 and Kashchiev, D (2022) Two-step crystal nucleation kinetics: Solution of the master equation. Journal of Crystal Growth, 580. 126469. ISSN 0022-0248

https://doi.org/10.1016/j.jcrysgro.2021.126469

Two-step crystal nucleation kinetics: solution of the master equation

Stefan Auer [a], Dimo Kashchiev [b,*]

[a] *School of Chemistry, University of Leeds, Leeds LS2 9JT, United Kingdom*

[b] *Institute of Physical Chemistry, Bulgarian Academy of Sciences, ul. Acad. G. Bonchev 11, Sofia 1113, Bulgaria*

A B S T R A C T

The master equation of two-step nucleation is numerically solved with parameters characterizing isothermal homogeneous nucleation of ice crystals and water droplets in steam below the water freezing temperature. The time dependences of the crystal and droplet size distributions and nucleation rates as well as of the nucleation rate of ice crystals in the droplets are determined at different constant supersaturations. The stationary values of these nucleation rates are obtained in a wide supersaturation range. It is found that when the crystallization of the water droplets is slower than their growth, the stationary rate of two-step crystal nucleation is orders of magnitude lower than the corresponding stationary rate of one-step crystal nucleation. As to the stationary nucleation rate of the water droplets, it is practically unaffected by the ice crystals nucleating and growing in both the droplets and the steam. Finally, the delay times of the different nucleation processes are determined and it is found that at both low and high supersaturations the delay time of the two-step crystal nucleation is negative because of the presence of high initial peak in the nonstationary rate of this process. The results obtained provide unprecedented mechanistic insight into the kinetics of two-step crystal nucleation.

* Corresponding author.

E-mail address: kash@ipc.bas.bg (D. Kashchiev).

1. Introduction

Crystal nucleation is a process whose understanding and control are of great academic and technological interest. In 1926, Volmer and Weber's pivotal paper [1] initiated the theoretical study of the kinetics of nucleation, and the results obtained in the following dozen or so years have come to be collectively known as the classical nucleation theory (CNT) (e.g., Refs. [2–4]). Regarding crystal nucleation, this theory is applicable when the crystals appear directly, i.e. in one step, in the supersaturated old phase (O-phase) by self-assembling of O-phase monomers (atoms or molecules or building blocks) into clusters of the thermodynamically stable crystal phase (C-phase). The only parameter used in CNT to distinguish these single-phase clusters from each other is the cluster size, i.e. the number of monomers constituting them.

Recently, however, compelling evidence has emerged from experiments, computer simulations and numerical studies (e.g., Refs. [5–34]) that crystals can often come into being by the so-called two-step (2S) nucleation in which the first step is the appearance of a thermodynamically metastable phase (M-phase) in the O-phase, and the second step is the crystal nucleation in this precursor M-phase. The theoretical description of 2S nucleation thus requires considering the appearance in the O-phase of two-phase clusters composed of two single-phase clusters, one of the M-phase, and the other of the C-phase. In the spirit of CNT, these composite clusters can be characterized by two cluster sizes: the total number i of monomers constituting the composite and the number n of monomers building-up the crystal cluster which is part of the composite ($n \leq i$). When these two sizes are equal, the composite cluster is identical with the crystal cluster used in CNT for description of one-step (1S) nucleation of crystals [2–4]. In this way, 1S nucleation appears merely as a limiting case of 2S nucleation.

Owing to this clear nexus between 1S and 2S nucleations, the composite-cluster model has been used to extend CNT in a way allowing the description of these two kinds of nucleation from a unified point of view [10,13,26,33,35–38]. In particular, in Ref. 38 the CNT master equation of 1S nucleation was generalized to apply to 2S nucleation by considering the process as evolving in the two-dimensional i,n space of the two cluster sizes, and general expressions were derived for the rates of 2S nucleation of crystals in the O-phase

and of crystal nucleation in the droplets. Mathematically, the master equation of 2S nucleation in Ref. 38 is of considerable complexity and it is not a simple matter to analytically obtain the time and supersaturation dependences of these nucleation rates. We still do not have the luxury to possess a sufficiently general analytical expression for the 2S nucleation rate, such as the exact Becker-Döring formula [39] for the rate of stationary 1S nucleation. In the absence of analytical results, the alternative is to employ numerical methods to solve the master equation with reference to a given nucleating system and thereby gain mechanistic insight into the idiosyncrasies of the kinetics of 2S nucleation.

The objective of the present study is thus to obtain a numerical solution of the master equation of 2S nucleation [38] with parameters corresponding to homogeneous nucleation of water droplets (the M-phase) and ice crystals (the C-phase) in steam (the O-phase) at a fixed temperature below the water freezing one. In particular, we find the size distributions of crystals, droplets, and composites as functions of time and use them for determination of the supersaturation dependence of the crystal and droplet nucleation rates and delay times, as well as for comparison of these dependences with those corresponding to 1S nucleation. The comparison of the nucleation rate of droplets involved in 2S nucleation with their rate corresponding to 1S nucleation is of special interest, because the nucleation of crystals in the droplets might be a factor in the well-documented discrepancy between CNT and experimental results for homogeneous nucleation of water droplets in steam below the water freezing temperature (e.g., Refs. [40–44]).

2. The master equation of 2S nucleation

We consider a supersaturated O-phase in which a single-component M-phase and the C-phase of the same component can nucleate homogeneously. The O-phase contains monomers that can directly self-assemble into M-phase or C-phase clusters by 1S nucleation as described by CNT (e.g., Ref. [4]). Alternatively, the O-phase can transform into C-phase indirectly, i.e. by 2S nucleation which involves appearance of M-phase clusters followed by nucleation of crystals in them. Most simply, 2S nucleation is thus characterized with the formation of i,n-sized clusters in the O-phase, each of them constituted of a single C-phase cluster of n monomers ($1 \le n \le i$) and a covering M-phase layer of $i-n$ monomers (Fig. 1a,

top). The more complicated case of two or more C-phase clusters nucleating in an M-phase cluster is not considered here. As i is the total number of monomers in the cluster, in the $n = i$ limit, the cluster is of size i,i and is an i-sized crystal in the O-phase because of the absence of M-phase layer around it (Fig. 1a, bottom left). In the opposite limit of $n = 1$, the cluster is of size $i,1$ and is an i-sized M-phase cluster (Fig. 1a, bottom right), because in CNT an $(n = 1)$-sized crystal in the M-phase is actually a monomer of the M-phase and is thus indistinguishable from the other monomers of the M-phase around it. To differentiate between the i,n-sized clusters in the O-phase, we shall hereafter call them M-phase clusters, composites, and crystals when $n = 1$, $1 < n < i$, and $n = i$, respectively. Correspondingly, the clusters of $n = 2,3,...,i-1$ monomers inside the composites will be referred to as crystals in the M-phase.

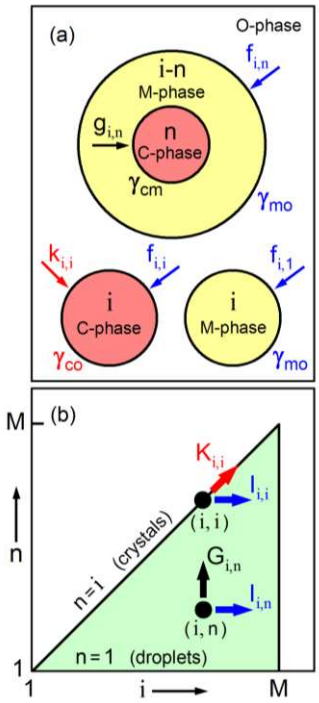

Fig. 1. (a) Schematic of composite cluster of i monomers with n-sized M-phase cluster in it (top), of crystal cluster of i monomers (bottom left) in O-phase, and of M-phase cluster of i monomers (bottom right) (the arrows illustrate the frequencies $f_{i,n}$, $g_{i,n}$, $f_{i,i}$, $k_{i,i}$ and $f_{i,1}$ of monomer attachment to the respective clusters). (b) The triangular i,n cluster-size space with the $I_{i,n}$, $G_{i,n}$, and $K_{i,i}$ fluxes (shown by arrows) that control the nucleation and growth of M-phase and composite clusters, of crystals in the M-phase, and of crystals in the O-phase,

respectively. The $I_{i,i}$ arrow visualizes the flux of i,i-sized crystals in the O-phase that transit to $i+1,i$-sized composites, and the circles represent points i,n and i,i in the size space.

The above is a compendious description of the composite-cluster model of CNT. In the framework of this model, the master equation of 2S nucleation is of the form [38] ($i = 3,4,...,M-1$, $n = 2,3,...,i-1$)

$$\frac{dZ_{i,n}(t)}{dt} = I_{i-1,n}(t) - I_{i,n}(t) + G_{i,n-1}(t) - G_{i,n}(t) . \quad (1)$$

Here $Z_{i,n}$ (m^{-3}) is the actual concentration of i,n-sized clusters at time t, and $I_{i,n}$ and $G_{i,n}$ are given by Eqs. (S1) and (S2) of Supplementary Material (SM). Also, $Z_{1,1} = C_1$ and $Z_{M,n}(t) = 0$ for any n [38], because the smallest clusters (for them $i = n = 1$) are identical with the O-phase monomers whose concentration is C_1 (m^{-3}) and because the formation of a cluster containing all M monomers of the O-phase is ruled out. As the crystal size n cannot exceed the cluster size i, the i,n cluster-size space in which 2S nucleation evolves is triangular (Fig. 1b). For the boundary lines $n = 1$ and $n = i$ of this space (Fig. 1b), instead of Eq. (1) we have [38] ($i = 2,3,...,M-1$)

$$\frac{dZ_{i,1}(t)}{dt} = I_{i-1,1}(t) - I_{i,1}(t) - G_{i,1}(t) \quad (2)$$

$$\frac{dZ_{i,i}(t)}{dt} = K_{i-1,i-1}(t) - K_{i,i}(t) + G_{i,i-1}(t) - I_{i,i}(t) \quad (3)$$

where $K_{i,i}$ is given by Eq. (S3) of SM.

Physically, the quantities $I_{i,n}$ and $G_{i,n}$ are the net rates at which the i,n-sized clusters become $i+1,n$-sized and $i,n+1$-sized, respectively, and $K_{i,i}$ is the net rate at which the i,i-sized crystals become $i+1,i+1$-sized. The rates $I_{i,n}$ and $G_{i,n}$ can be regarded as fluxes flowing from point i,n in the two-dimensional cluster-size space to point $i+1,n$ and to point $i,n+1$, respectively, which means that whereas $I_{i,n}$ is parallel to the i-axis, $G_{i,n}$ is parallel to the n-axis of this space (Fig. 1b). Likewise, $K_{i,i}$ is the flux flowing from point i,i to point $i+1,i+1$ on the diagonal boundary line $n = i$ of this space (Fig. 1b). The particular cases of (i) $I_{i,n} = G_{i,n} = 0$ for all i,n, (ii) $K_{i,i} = G_{i,n} = 0$ for all i,n and $I_{i,n} = 0$ for $i \geq 2$, $n = 2,3,...,i$, and (iii) $G_{i,n} = 0$ for all i,n and $I_{i,n} = 0$ for $i \geq 2$, $n = 2,3,...,i$ correspond, respectively, to 1S

nucleation of crystals on the $n = i$ line [4], to 1S nucleation of M-phase clusters on the $n = 1$ line [4], and to simultaneous occurrence of these two processes [45].

According to Eqs. (S1)–(S3) of SM, the $I_{i,n}$, $G_{i,n}$ and $K_{i,i}$ fluxes depend strongly on the cluster formation work $W_{i,n}$, because the equilibrium cluster concentration $C_{i,n}$ determining them is related to $W_{i,n}$ by the Boltzmann-type formula [38] ($i = 1,2,3,...$, $n = 1,2,3,...,i$)

$$C_{i,n} = C_1 \exp(w_{1,1} - w_{i,n}) . \quad (4)$$

Here C_1 is the concentration of monomers in the O-phase, $w_{i,n} \equiv W_{i,n} / k_B T$ is the dimensionless work to form an i,n-sized cluster, k_B is the Boltzmann constant, T is the absolute temperature of the system, and $w_{1,1}$ is the value of $w_{i,n}$ at $i = n = 1$. Eq. (4) is self-consistent in the sense that at $i = n = 1$ it returns the equality $C_{1,1} = C_1$. Also, it is general and can be used with any model for $w_{i,n}$. Hereafter, we shall use the expression [38] ($i = 1,2,3,...$, $n = 1,2,3,...,i$, $s_{co} > s_{cm} > 0$)

$$w_{i,n} = -(s_{co} - s_{cm})i + \gamma_{mo} i^{2/3} - s_{cm} n + \gamma_{cm} n^{2/3} \quad (5)$$

where $s_{co} - s_{cm} = s_{mo}$ is the dimensionless supersaturation of the O-phase with respect to the M-phase, s_{co} is the dimensionless supersaturation of the O-phase with respect to the C-phase, s_{cm} is the dimensionless supersaturation of the M-phase with respect to the C-phase, γ_{mo} is the dimensionless M-phase/O-phase specific surface energy, and γ_{cm} is the dimensionless C-phase/M-phase specific surface energy. In the case when the O-phase is a single-component vapor behaving as ideal gas, the three s's are given by Eq. (S6) of SM, and expressions for them in the case of O-phase which is a single-component melt are presented elsewhere [38, 46]. It is important to note that s_{cm} is independent of s_{co} in the former case provided s_{co} is changed via the pressure of the gaseous O-phase. Under the assumption that both the M-phase and the C-phase clusters are spherical, γ_{mo}, γ_{cm} and the dimensionless C-phase/O-phase specific surface energy γ_{co} are given by Eqs. (S7) and (S9) of SM and are related by the simple equality [38] $\gamma_{co} = \gamma_{cm} + \gamma_{mo}$.

Eq. (5) corresponds to the simplest CNT-inspired version of the composite-cluster model [38], in which (i) the interaction between the two surfaces of the composite cluster (Fig. 1a) is not taken into account, (ii) the possible i,n dependences of γ_{mo} and γ_{cm} are ignored, and (iii) the monomer volume is considered as being the same in both the M-phase

and the C-phase. A more elaborate version of the model is the one with relaxed point (i) only (e.g., Refs. [33] and [35]). This version makes it possible to account for such important phenomena as adsorption, wetting, and surface melting that may occur on the surface of the crystals in the O-phase. Additionally relaxing points (ii) and (iii) is also of interest, the point (iii) relaxation being of particular interest in 2S nucleation in which the M- and O-phases are crystal polymorphs.

Besides thermodynamics (via $w_{i,n}$), kinetics is also involved in the $I_{i,n}$, $G_{i,n}$ and $K_{i,i}$ fluxes through the attachment frequencies $f_{i,n}$, $g_{i,n}$ and $k_{i,i}$ (Fig. 1a) of, respectively, monomers of the O-phase to an i,n-sized composite, monomers of the M-phase layer of such a composite to the n-sized crystal in it, and monomers of the O-phase to an i-sized crystal in the O-phase (i.e. an i,i-sized cluster) which transform this crystal into a crystal of size $i+1$. For the simplest version of the composite-cluster model used here, provided all monomers arriving at the cluster surface are attached to the cluster, we can approximate the i,n dependence of these frequencies by the CNT expressions for 1S nucleation which are presented by Eqs. (S10)–(S12) of SM. These expressions correspond to the case of monomer attachment to the clusters in the gaseous O-phase by direct impingement onto the cluster surface and to monomer attachment to the crystals within the composites by interface-transfer control.

When the O-phase is held at constant monomer concentration C_1 and temperature T, the supersaturation s_{co} and the equilibrium cluster concentration $C_{i,n}$ are time-independent. Then, as shown in Section S2 of SM, Eqs. (1)–(3) can be amalgamated into a single equation of the form ($i = 2,3,...,M-1$, $n = 1,2,...,i$)

$$\frac{dF_{i,n}}{dx} = a_{i,n}(F_{i-1,n} - F_{i,n}) - b_{i,n}(F_{i,n} - F_{i+1,n}) + c_{i,n}(F_{i,n-1} - F_{i,n}) \\ - d_{i,n}(F_{i,n} - F_{i,n+1}) + e_{i,n}(F_{i-1,i-1} - F_{i,i}) - h_{i,n}(F_{i,i} - F_{i+1,i+1}) . \qquad (6)$$

Here the dimensionless cluster concentration $F_{i,n} \geq 0$ and time $x \geq 0$ are given by

$$F_{i,n}(x) = \frac{e^{\Delta w_{i,n}} Z_{i,n}(x)}{C_1}, \quad x = f_0 t \qquad (7)$$

where the quantity $\Delta w_{i,n}$ is defined as $\Delta w_{i,n} \equiv w_{i,n} - w_{1,1}$, and the frequency factor f_0 (s^{-1}) is specified by Eq. (S13) of SM. Physically, the x-independent coefficients $a_{i,n}$, $c_{i,n}$ and $e_{i,n}$ in

Eq. (6) are the dimensionless, normalized by f_0, frequencies of monomer detachment from both the M-phase clusters and the composites (coefficient $a_{i,n}$), from the crystals within the composites (coefficient $c_{i,n}$), and from the crystals in the O-phase (coefficient $e_{i,n}$). Similarly, $b_{i,n}$, $d_{i,n}$ and $h_{i,n}$, also x-independent, are the dimensionless frequencies of monomer attachment to both the M-phase clusters and the composites, to the crystals within the composites and to the crystals in the O-phase, respectively. The general expressions for these six attachment/detachment frequencies, which are valid for any model of 2S nucleation thermodynamics ($w_{i,n}$) and kinetics ($f_{i,n}$, $g_{i,n}$ and $k_{i,i}$), are Eqs. (S19)–(S24) of SM. The specific expressions corresponding to our model for $w_{i,n}$, $f_{i,n}$, $g_{i,n}$ and $k_{i,i}$, and used by us, are Eqs. (S25)–(S31) of SM.

In addition to the master Eq. (6), for $F_{1,1}$ and $F_{M,n}$ we have the boundary conditions $F_{1,1}(x) = 1$ and $F_{M,n}(x) = 0$ (for $n = 1,2,...,M$), because $\Delta w_{1,1} = 0$ and $Z_{1,1} = C_1$ in Eq. (7), and because $Z_{M,n}(t) = 0$ for any size n. As Eq. (6) is a set of $(M/2)(M-1)-1$ linear ordinary differential equations of first order for the same number of unknowns $F_{i,n}$, the problem of finding $F_{i,n}$ becomes mathematically well-posed when the initial concentration of the clusters is specified. In the present study, we shall use the initial condition $F_{i,n}(0) = 0$ (for $i = 2,3,...,M$, $n = 1,2,...,i$) which corresponds to 2S nucleation commencing in the absence of clusters in the system.

3. Numerical solution of the master equation

3.1 Parameter values

Our task is to numerically solve the master Eq. (6) for $F_{i,n}(x)$ when this quantity satisfies the conditions for $F_{1,1}(x)$, $F_{M,n}(x)$ and $F_{i,n}(0)$ noted above and when the attachment/detachment frequencies from Eqs. (S25)–(S31) of SM are approximately relevant to homogeneous nucleation of water droplets (the M-phase) and ice crystals (the C-phase) in steam (the O-phase) at temperature $T \approx 220-230$ K and of ice crystals in liquid water at the same temperature. As shown in Section S3 of SM, in this case, we have $s_{cm} = 0.5$, $\gamma_{mo} = 12.8$, $\gamma_{cm} = 2.6$, $\gamma_{co} = 15.4$, $f_0 = 10^5$ s^{-1}, $C_1 = 1.6\times10^{21} e^{s_{co}}$ m^{-3}, and $L = 200$. This

value of the parameter L in Eqs. (S28) and (S29) of SM means that when s_{co} is sufficiently small, monomer attachment to an n-sized ice crystal inside a water composite of $i > n$ monomers can be much faster than that to the liquid layer of the composite or to an i-sized droplet as long as i is not too much greater than n (see Eqs. (S10)–(S12) of SM). As to the parameter Q in Eqs. (S25), (S27), (S30) and (S31) of SM, its value is unknown and we choose $Q = 1/2$, the value corresponding to equal frequencies $f_{i,i}$ and $k_{i,i}$ of monomer attachment to the ice crystals in the steam (according to Eqs. (S10) and (S12) of SM). By using $Q < 1/2$ or $Q > 1/2$, one could account for growth of the i,i-sized crystals to $i+1,i+1$-sized ones which is, respectively, impeded or facilitated in comparison with the transition of the crystals to $i+1,i$-sized composites.

Using the above parameter values and the attachment/detachment frequencies from Eqs. (S25)–(S31) of SM, we numerically obtained first $F_{i,n}(x)$ from Eq. (6) and then, with its help, the concentration of i,n-sized clusters as well as the nucleation rates and number densities of crystals, composites and droplets at ten values of the supersaturation s_{co} in the range from 2 to 6. This range is of interest, because experiments on homogeneous nucleation of water droplets in steam at 220 and 230 K have been carried out at s_{mo} from about 1.8 to 3.3 (e.g., Refs. [40–44]; see also Fig. 5 of Ref. [47]), which corresponds to $s_{co} = 2.3$ to 3.8.

3.2. Numerical method

To obtain the results reported below, we used $M = 240$. This M value requires the numerical solution of $(M/2)(M-1)-1 = 28679$ simultaneous ordinary differential equations, and this large number prohibited us from employing a considerably greater M. The finite-size effect due to the use of our M value is discussed and illustrated in SM. For the numerical solving of our large set of equations we employed the odeint (ordinary differential equation integration) open source library [48]. It contains a function that computes the $F_{i,n}(x)$ derivative in accordance with Eq. (6) and the conditions for $F_{1,1}(x)$, $F_{M,n}(x)$ and $F_{i,n}(0)$ noted above, and provides a sequence of x values at which to solve for $F_{i,n}(x)$. For our calculations we used the odeint default parameters, except that for $s_{co} > 2.2$ we had to restrict the maximum absolute step size allowed with regard to x. A point to note also is that, as the

computation of the nucleation rates requires integer values for the nucleus sizes i^*, n^* and i_{co}^*, a non-integer nucleus size was always rounded off to the nearest upper integer size.

4. Results and discussion

4.1. Energy landscape

The cluster formation work $w_{i,n}$ determines the energy landscape of the 2S nucleation process. According to Eq. (5), $w_{i,n}$ has a maximum at point i^*,n^* in the i,n cluster-size space. The i^*,n^*-sized cluster is the composite nucleus, and i^* and n^* are given by the Gibbs-Thomson equations [38] $i^* = [2\gamma_{mo}/3(s_{co} - s_{cm})]^3$ and $n^* = (2\gamma_{cm}/3s_{cm})^3$ in which $s_{co} > s_{cm} > 0$. These equations show that while i^* decreases strongly with increasing s_{co}, n^* is s_{co}-independent (for our parameter values, $i^* = 185$ to 4 for s_{co} from 2 to 6, and $n^* = 42$). Importantly, as in our study the interaction between the crystal/M-phase and M-phase/O-phase interfaces of the composite is neglected, i^* is also the size of the M-phase nucleus, and n^* is also the size of the crystal nucleus in the bulk M-phase.

The three-dimensional $w_{i,n}$ function from Eq. (5) is dome-shaped. In two dimensions, the set of borderlines between the concentric ellipsoidal strips in Fig. 2 represents the 2S nucleation energy landscape (the $w_{i,n} = \text{constant}$ contour plot) when $w_{i,n}$ is specified by our parameter values. The stars mark the position of the (i^*,n^*)-sized composite nucleus in the cluster size space and designate the peak of $w_{i,n}$ at $s_{co} = 2.5$ (Fig. 2a), $s_{co} = 3$ (Fig. 2b), and $s_{co} = 5$ (Fig. 2c). The concentric contour-plot lines connect the i,n values at which $w_{i,n}$ has a given value smaller than its maximum value $w^* \equiv w_{i^*,n^*}$ (the farther a line from the center, the smaller the $w_{i,n}$ value corresponding to it). The two $i = i^*$ and $n = n^*$ ridges of the $w_{i,n}$ energy hill, which have to be surmounted by the subnucleus clusters when they grow parallel to the n- or i-axis, are visualized by the vertical and the horizontal straight lines, respectively. The upper triangular part of the contour plot in each panel of Fig. 2 is obscure, because it is in the physically inaccessible i,n cluster size space.

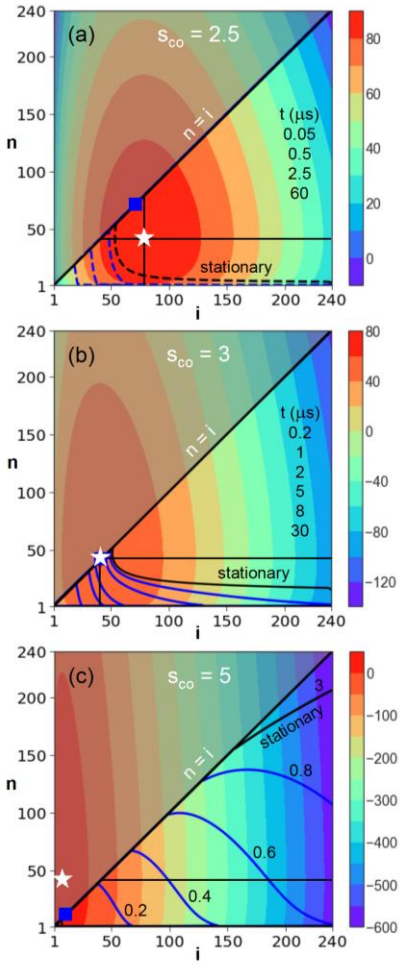

Fig. 2. Contour plot (the borderlines between the ellipsoidal strips) of the cluster formation work $w_{i,n}$ from Eq. (5) with superimposed front of the cluster concentration $Z_{i,n}$ from Eq. (8) at successive times (indicated in μs) of 2S nucleation when (a) $s_{co} = 2.5$ (then $i^* > n^*$), (b) $s_{co} = 3$ (then $i^* \approx n^*$), and (c) $s_{co} = 5$ (then $i^* < n^*$). The concentration of i,n-sized clusters on a front line at any time t is $Z_{i,n}(t) = 1$ km^{-3} in panel (a), 1 m^{-3} in panel (b) and 1 mm^{-3} in panel (c). In each panel, the star visualizes the position i^*,n^* of the $w_{i,n}$ maximum, the square on the $n = i$ line indicates the size i_{co}^* of the ice crystal nucleus in the steam, and the vertical and horizontal lines represent the i^* and n^* ridges of the $w_{i,n}$ surface, respectively. The $w_{i,n}$ scale is on the right of the panels.

Regardless of whether the crystals in the supersaturated O-phase come into being by 1S or 2S nucleation, they are viable only after surpassing the nucleus size i_{co}* indicated by the square on the $n = i$ diagonals in Fig. 2. This size is determined by the Gibbs-Thomson equation [38] $i_{co}^* = (2\gamma_{co}/3s_{co})^3$ according to which, for our γ_{co} value, $i_{co}^* = 136$ to 5 for s_{co} from 2 to 6. Thus, while at low supersaturation the ice crystal nucleus in steam is smaller than the composite (or the droplet) nucleus, at high supersaturation it is larger. We note as well that the energy landscape in Fig. 2 is so simple, because Eq. (5) describes $w_{i,n}$ in perhaps the simplest possible way. When composite-cluster surface interaction or specific molecular interactions are taken into account, this landscape can be quite complicated, because then the $w_{i,n}$ surface can have saddle point(s) and more than one maximum in the physically accessible cluster size space (e.g., Refs. [17,18,32–35]). In our case, due to the absence of surface-interaction term in Eq. (5), the saddle points that characterize $w_{i,n}$ when this term is present [33,35] appear on the boundaries of the cluster size space (the $n = i$ and $n = 1$ lines in Fig. 2).

4.2. Cluster size distribution

When $F_{i,n}$ is known, according to Eq. (7), the cluster concentration $Z_{i,n}$ can be obtained from

$$Z_{i,n}(x) = C_1 e^{-\Delta w_{i,n}} F_{i,n}(x). \qquad (8)$$

In the triangular cluster-size space of 2S nucleation, the curved lines in Figs. 2a–2c illustrate the spreading of the front of the cluster concentration from Eq. (8) for supersaturations $s_{co} = 2.5$, 3 and 5 at which $i^* > n^*$, $i^* \approx n^*$ and $i^* < n^*$, respectively. This front is defined as the line connecting those *i*,*n* points that at a given time *t* represent the sizes of the clusters with concentration $Z_{i,n}(t) = 1$ km^{-3} (for Fig. 2a), 1 m^{-3} (for Fig. 2b), and 1 mm^{-3} (for Fig. 2c). In each panel, the rightmost line visualizes the static front when the 2S nucleation is stationary, and the lines on the left of it show the front at previous times at which the process is still transient. The leftmost lines in the panels correspond to the earliest times, and while in panels (a) and (b) the successive times (in μs) are listed in a column, in panel (c) they are indicated by numbers at the lines.

As seen in Fig. 2, the stationary cluster concentration fronts are distinctly different when the starred peak of the energy hill is inside or outside the physically accessible cluster-size triangle. In the former case (Fig. 2a, $i^* > n^*$), the front circumvents the energy peak, because the clusters grow predominantly parallel either to the $n = i$ diagonal or to the $n = 1$ line. These two roundabout pathways correspond to 1S nucleation of ice crystals and of water droplets, respectively. In the latter case (Fig. 2c, $i^* < n^*$), the absence of the energy peak allows almost unhindered cluster growth parallel to the $n = 1$ line. This means prevailing nucleation of droplets and composites whose subsequent crystallization yields 2S-nucleated ice crystals in the steam. In the demarcating $i^* \approx n^*$ case (Fig. 2b, energy peak practically on the $n = i$ diagonal), the stationary front is like that in the $i^* > n^*$ case (Fig. 2a), but considerably more extended toward the larger droplets and composites.

The size distributions of ice crystals ($Z_{i,i}$) and water droplets ($Z_{i,1}$) in the steam at successive times (as indicated) are depicted in Figs. 3a–3c and Figs. 3d–3f, respectively. Similarly, Figs. 3g–3i and Figs. 3j–3l display the evolution of the size distribution Z_{i,n^*} of those water composites of $i > n^*$ monomers that contain an n^*-sized ice crystal nucleus, and the evolution of the size distribution $Z_{i^*,n}$ of ice crystals within those composites that, like the droplet nucleus, are constituted of i^* monomers. These two size distributions are the $Z_{i,n}(t)$ values along the n^* and the i^* ridges of the $w_{i,n}$ surface, respectively (the horizontal and the vertical lines in Figs. 2a–2c). In Fig. 3, the panels on the left, in the middle and on the right refer to $s_{co} = 2.5$, 3 and 5, respectively.

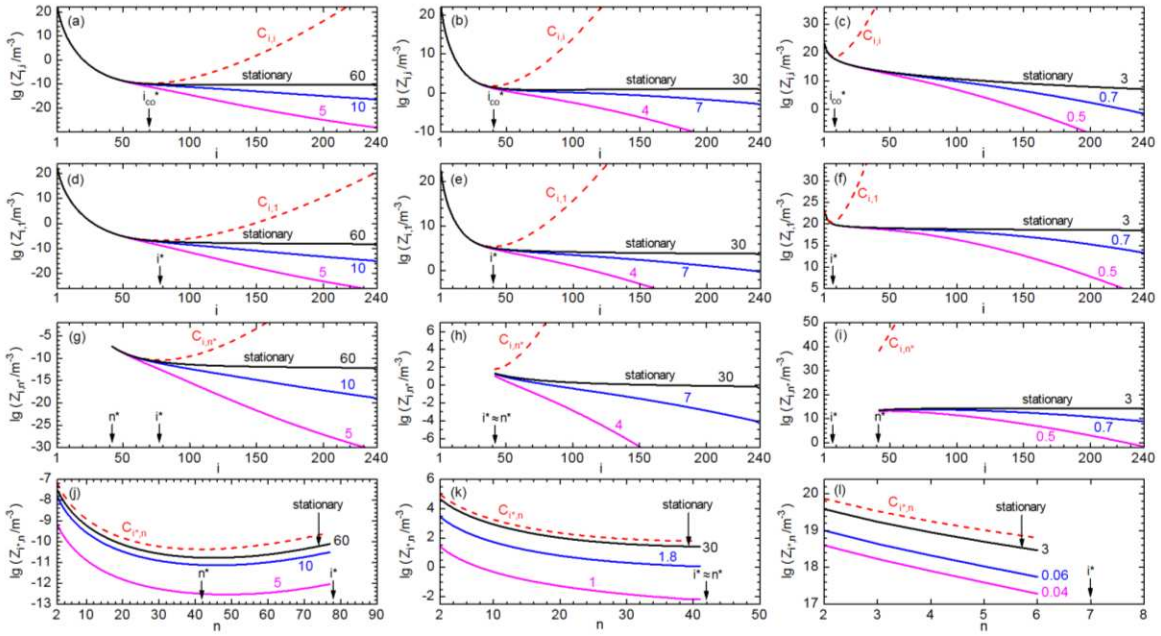

Fig. 3. Cluster size distributions from Eq. (8) at $s_{co} = 2.5$ (left column of panels), $s_{co} = 3$ (middle column of panels), and $s_{co} = 5$ (right column of panels). $Z_{i,i}$, $Z_{i,1}$, Z_{i,n^*}, and $Z_{i^*,n}$ refer, respectively, to ice crystals in steam, water droplets, water composites containing the n^*-sized ice crystal nucleus, and ice crystals within those composites that are with the size i^* of the droplet nucleus. The numbers at the lines indicate the time (in μs) elapsed from the onset of the 2S nucleation process. The dashed lines represent the corresponding equilibrium cluster size distributions $C_{i,i}$, $C_{i,1}$, C_{i,n^*}, and $C_{i^*,n}$ from Eq. (4).

In Fig. 3, all equilibrium cluster size distributions (dashed lines) are seen to quite closely approximate the respective stationary ones for the $i < i_{co}^*$-sized ice crystal subnuclei in the steam and for the droplet and composite subnuclei of size $i < i^*$, i.e. for the clusters on the left of the i^* ridge in Fig. 2. In this, these distributions are similar to the CNT equilibrium cluster size distribution in 1S nucleation (Ref. [4], Fig. 13.1). Also like in CNT, the above three kinds of subnuclei and nuclei are formed almost immediately after the onset of the 2S nucleation process. The distributions with respect to the cluster size i (panels (a)–(i) of Fig. 3) decrease monotonically with this size, except for Z_{i,n^*} (the composites on the n^* ridge in

Fig. 2) which increases at $s_{co} = 5$ (Fig. 3i), because at high supersaturations the predominant spreading of the cluster concentration front parallel to the *i* axis involves more and more composites with $n \geq n^*$-sized crystal nuclei and supernuclei in them (see line "stationary" in Fig. 2c). As to the size distribution $Z_{i^*,n}$ of composites on the i^* ridge in Fig. 2, Figs. 3j and 3k show that those composites that contain the n^*-sized ice crystal nucleus (i.e. those atop the energy peak in Figs. 2a and 2b) are the least populated species. The reason for that is the avoidance of the energy peak by the growing clusters which follow the two available roundabout pathways near the $n = i$ diagonal and the $n = 1$ line.

4.3. Net cluster fluxes

When the solution $F_{i,n}(x)$ of Eq. (6) is known, according to Eq. (8) and to Eqs. (S1)–(S3) of SM, the three fluxes $I_{i,n}$, $G_{i,n}$ and $K_{i,i}$ (in units of m^{-3} s^{-1}) can be obtained from the expressions

$$I_{i,n}(t) = f_0 C_1 b_{i,n} e^{-\Delta w_{i,n}} (F_{i,n} - F_{i+1,n}) \tag{9}$$

$$G_{i,n}(t) = f_0 C_1 d_{i,n} e^{-\Delta w_{i,n}} (F_{i,n} - F_{i,n+1}) \tag{10}$$

$$K_{i,i}(t) = f_0 C_1 h_{i,i} e^{-\Delta w_{i,i}} (F_{i,i} - F_{i+1,i+1}). \tag{11}$$

These fluxes determine the trajectories of cluster growth in the triangular cluster-size space of 2S nucleation. The arrowed cluster flow lines seen in Fig. 4 are a revealing visualization of these trajectories at $s_{co} = 2.5$, 3 and 5 (as indicated) and at $t = 60$ μs (Fig. 4a), 30 μs (Fig. 4b) and 3 μs (Fig. 4c) when the 2S crystal nucleation is already stationary. The lines are plotted with the help of the streamplot function available in the matplotlib library [49], and each line is drawn so that its tangent and direction at any point *i*,*n* are given by the vector sum of the fluxes $I_{i,n}$ and $G_{i,n}$ (if $n < i$) or the fluxes $I_{i,i}$ and $K_{i,i}$ (if $n = i$) considered as vectors beginning at this point (see Fig. 1b).

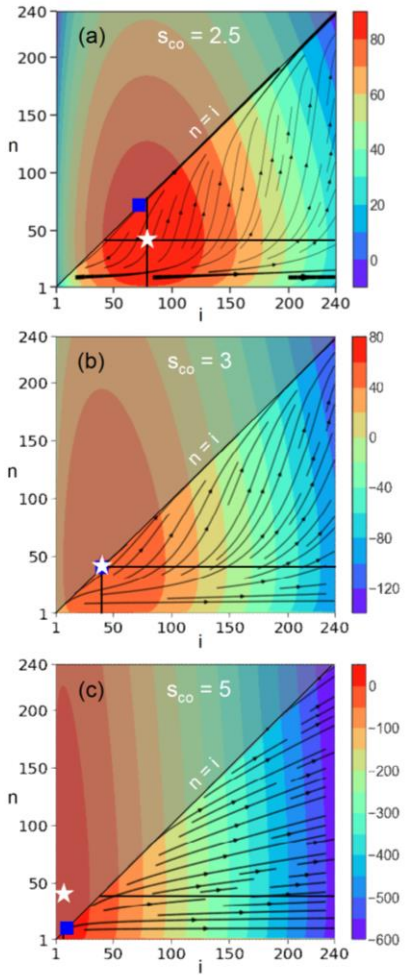

Fig. 4. Cluster flow lines dictated by the fluxes from Eqs. (9)–(11) in stationary 2S nucleation when: (a) $s_{co} = 2.5$, (b) $s_{co} = 3$, and (c) $s_{co} = 5$ (then $i^* > n^*$, $i^* \approx n^*$, and $i^* < n^*$, respectively). The arrow heads indicate the flow direction, and the background is the $w_{i,n}$ contour plot from Fig. 2. In each panel, the star visualizes the position i^*,n^* of the $w_{i,n}$ maximum, the square on the $n = i$ line indicates the size i_{co}^* of the ice crystal nucleus in the steam, the vertical and horizontal lines represent the i^* and n^* ridges of the $w_{i,n}$ surface, respectively, and the upper triangular part of the contour plot is obscure, because it is in the physically inaccessible i,n cluster size space. The $w_{i,n}$ scale is on the right of the panels.

The cluster flow lines in Fig. 4a show clearly that when $i^* > n^*$ so that the energy peak (the star) is inside the physically accessible triangular cluster-size space, in trying to circumvent the peak during their growth, the $i < i^*$-sized subnucleus composites predominantly take the two available roundabout pathways toward the $n = i$ diagonal of the ice crystals in steam and toward the $n = 1$ line of the water droplets. Once overcoming the vertical energy ridge in Fig. 4a and thus becoming supernuclei of size $i > i^*$, all composites with an $n > n^*$-sized crystal supernucleus in them (they are above the horizontal energy ridge in Fig. 4a) begin crystallizing, which is evidenced by the turning of the flow lines toward the $n = i$ diagonal and their merging with the flow line on this diagonal. Thus, the 2S-nucleated ice crystals contribute to the crystals formed by 1S nucleation on the $n = i$ diagonal. This mixed 1S-2S nucleation takes place even when the energy peak is practically on this diagonal (then $i^* \approx n^*$) despite that then growth parallel to the i axis is the only pathway for the composites to avoid the peak: as revealed in Fig. 4b, then the 2S-nucleated ice crystals again contribute to the 1S-nucleated ones because of the merging of their flow lines with the flow line on the $n = i$ diagonal. The situation is diametrically different, however, when $i^* < n^*$ so that the energy peak is outside the cluster size space of 2S nucleation. In Fig. 4c we observe that instead of joining the $n = i$ diagonal, now flow lines are leaving it, which means that many 1S-nucleated crystals become composites. Thus, rather than a contribution of 2S-nucleated crystals to the 1S-nucleated ones, there is now a loss of the latter. This effect is of general character and can manifest itself at high enough supersaturations when the droplet crystallization is slower than the crystal transition to composites and/or the growth of the composites and the droplets. Even at such supersaturations, however, cessation or at least a sufficient retardation of the latter two processes would ultimately lead to the droplet crystallization. As shown elsewhere [50], all droplets nucleate crystals in the O-phase also in the limiting case of infinitely fast growth of the supernucleus crystals inside them. We note as well that, as seen in Fig. S8 of SM, the subnucleus composites grow very chaotically before becoming sufficiently large.

4.4. Nonstationary nucleation rates

Knowing the three fluxes $I_{i,n}$, $G_{i,n}$ and $K_{i,i}$, we can determine various nucleation rates that characterize 2S and 1S nucleations [38]. In Fig. 5 we present only five of them: the rates J_c and $J_{c,1S}$ of 2S and 1S nucleations of $i > i_{co}*$-sized ice crystals in the steam, the rate $J_{c,d}$ of nucleation of $n > n*$-sized ice crystals in the droplets, the rate J_d of nucleation of $i > i*$-sized droplets during 2S crystal nucleation in the steam (called hereafter the rate of 2S droplet nucleation), and the rate $J_{d,1S}$ of 1S droplet nucleation. Other three nucleation rates (of composites, of droplets plus composites, and of droplets plus composites plus crystals) are presented in Fig. S1 of SM. The rate $J_{c,1S}$ is obtained from the solution of Eq. (6) at $Q = 1$ and $a_{i,n}$, $b_{i,n}$, $c_{i,n}$, and $d_{i,n}$ set equal to zero, and corresponds to the CNT 1S process of droplet-unaffected crystal nucleation in the one-dimensional cluster-size space of the $n = i$ diagonal in Fig. 1b. Similarly, the rate $J_{d,1S}$ is obtained from the solution of Eq. (6) at annulled Q, $c_{i,n}$, $d_{i,n}$, $e_{i,n}$, and $h_{i,n}$. This is the rate of the CNT 1S process of crystal-unaffected droplet nucleation in the one-dimensional cluster-size space of the i axis in Fig. 1b (then no ice crystals nucleate in either the steam or the droplets). The rates displayed in Fig. 5 are calculated from the equations [38]

$$J_c(t) = K_{i_{co}*,i_{co}*} + \sum_{i=i_{co}*+1}^{M-1}(G_{i,i-1} - I_{i,i}) \tag{12}$$

$$J_{c,d}(t) = \sum_{i=n*+1}^{M-1} I_{i,i} + \sum_{i=n*+2}^{M-1}(G_{i,n*} - G_{i,i-1}) \tag{13}$$

$$J_d(t) = I_{i*,1} - \sum_{i=i*+1}^{M-1} G_{i,1} \tag{14}$$

and from Eqs. (S35) and (S36) of SM.

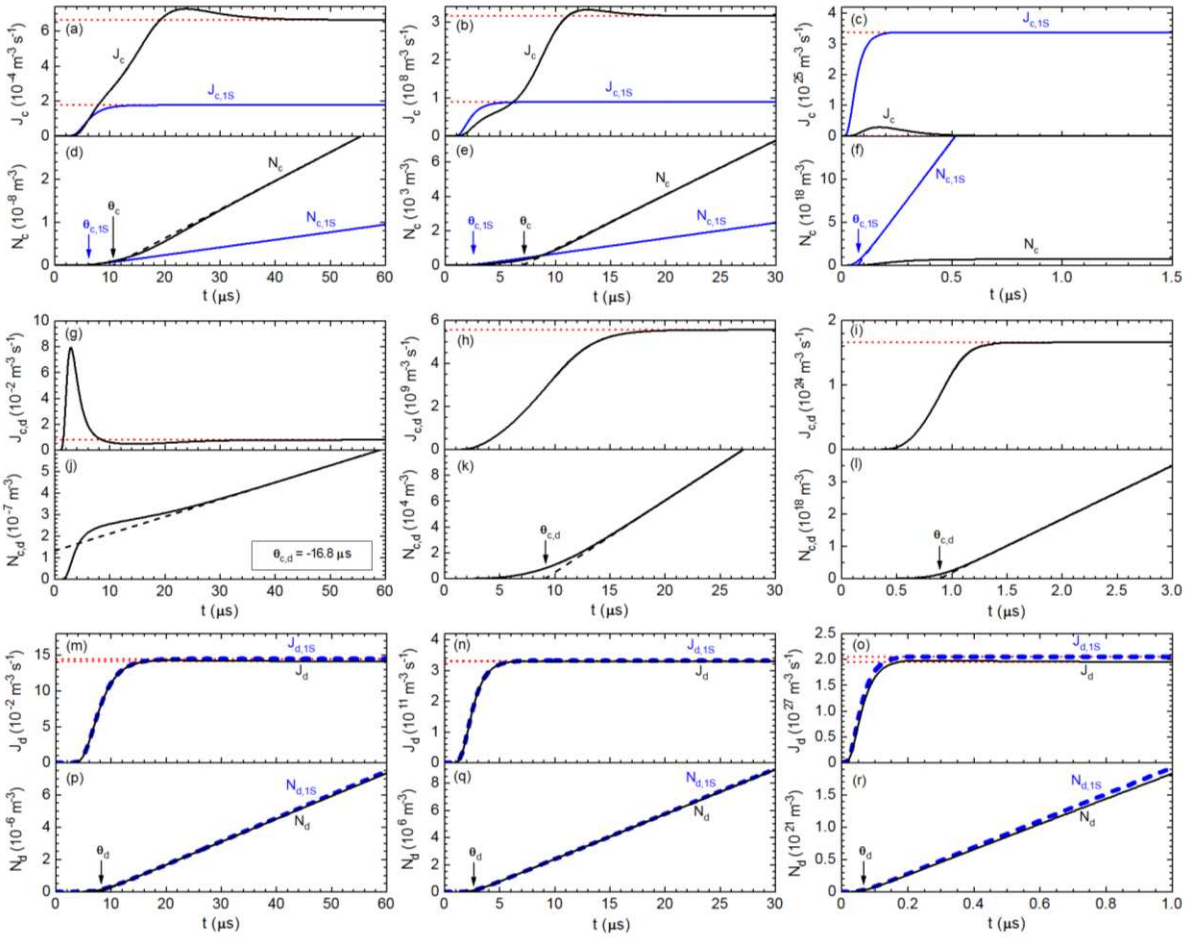

Fig. 5. Time dependence of the nucleation rates J and the number densities N of supernuclei from Eqs. (12)–(14) and from Eqs. (S35), (S36), (S41) and (S42) of SM at $s_{co} = 2.5$ (left column of panels), $s_{co} = 3$ (middle column of panels), and $s_{co} = 5$ (right column of panels). The dotted lines in the $J(t)$ panels represent the respective stationary nucleation rates, the thin dashed lines in the $N(t)$ panels are the long-time $N(t)$ asymptotes, and the arrows in these panels indicate the respective delay times of nucleation.

We first consider the nonstationary 2S and 1S crystal nucleation rates J_c and $J_{c,1S}$ displayed by the solid lines in Figs. 5a–5c. As expected, the rate $J_{c,1S}$ has the sigmoidal shape known from CNT [4]. As to J_c, as seen, it is a complicated function of time, which passes

through a maximum before acquiring its stationary value. This value exceeds that of $J_{c,1S}$ at $s_{co} = 2.5$ and 3 (Figs. 5a and 5b), but at $s_{co} = 5$ (Fig. 5c) its smallness, 3.35×10^{15} m^{-3} s^{-1}, makes it indistinguishable from the zero on the J_c axis. Thus, while at the lower supersaturations the stationary 2S nucleation of crystals occurs at a rate which is higher than that of 1S crystal nucleation, the opposite is true at higher supersaturations. Looking back at Fig. 4 which refers to stationary 2S nucleation, we see that, indeed, whereas at $s_{co} = 2.5$ and 3 the ice crystals nucleated in the droplets add to the 1S-nucleated ice crystals in the steam, at $s_{co} = 5$, for the already noted kinetic reason of both the crystal-to-composite transition and the composite and droplet growth faster than their crystallization, many initially 1S-nucleated crystals are lost after becoming composites so that, overall, less ice crystals are nucleated in the steam.

The nonstationary rate $J_{c,d}$ of ice crystal nucleation in the droplets (the solid lines in Figs. 5g–5i) is also of interest. We observe that the maximum of the $J_{c,d}(t)$ dependence at small s_{co} disappears when s_{co} is large. The reason is that while at $s_{co} = 2.5$ some of the initially rapidly appearing $i < i^*$-sized subnucleus droplets are of size $i > n^*$ and are thus able to give birth to $n > n^*$-sized crystal supernuclei in them (the process manifested by the $J_{c,d}$ maximum in Fig. 5g), at $s_{co} = 3$ and 5 this is impossible, because all these droplets have size $i < n^*$, i.e. they are smaller than the crystal supernuclei that are to appear in them. Indeed, whereas $i^* = 78$, 40 and 7 at $s_{co} = 2.5$, 3 and 5, respectively, $n^* = 42$ for all supersaturations.

Finally, we turn to the J_d and $J_{d,1S}$ time dependences graphed, respectively, by the solid and dashed lines in Figs. 5m–5o. We see that apart from its initial negligible maximum, J_d has the $J_{d,1S}$ sigmoidal shape predicted by CNT [4]. Seen also in these figures is that J_d differs slightly from $J_{d,1S}$ only at the long enough times when nucleation is already stationary. This insignificant difference is an important finding, because within the caveats of our model for cluster formation work and attachment/detachment frequencies, Eq. (5) and Eqs. (S10)–(S12) of SM, it indicates that the homogeneous nucleation of water droplets in steam in the temperature range $T \approx 220 - 230$ K considered here is practically unaffected by the nucleation of ice crystals in the droplets and the steam.

4.5. Stationary nucleation rates

As known [4], the stationary nucleation rate J^s is the $t \to \infty$ value of the respective time-dependent nucleation rate J (see the dotted lines in Fig. 5) and depends on the supersaturation s_{co}. In accordance with this definition, from our numerical $J(t)$ data for the longest computation time at each s_{co} value, we obtained the stationary nucleation rates J_c^s, $J_{c,1S}^s$, $J_{c,d}^s$, J_d^s, and $J_{d,1S}^s$ which are illustrated in Fig. 6 as functions of s_{co}. Other three $J^s(s_{co})$ dependences (for composites, for droplets plus composites, and for droplets plus composites plus crystals) are presented in Fig. S2 of SM. Numerically, the data for all stationary nucleation rates are given in Table S1 of SM.

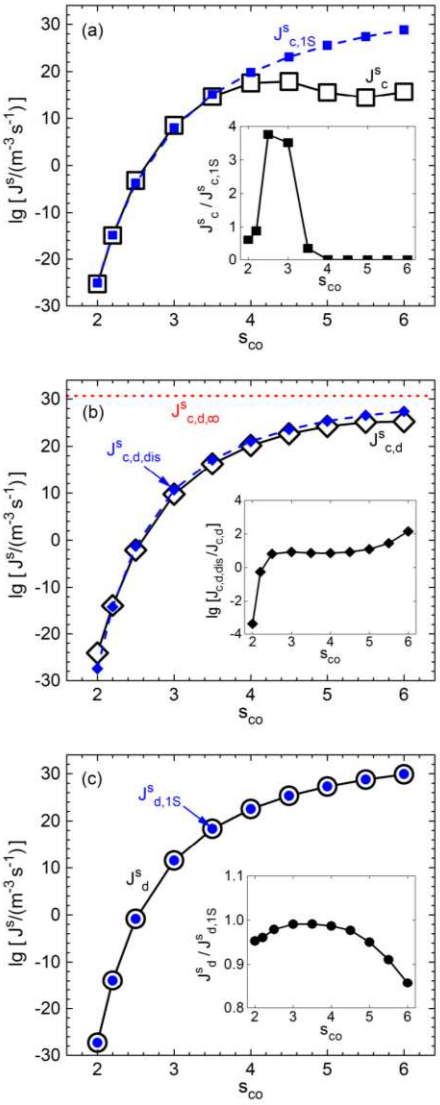

Fig. 6. Supersaturation dependence of stationary nucleation rate: (a) J_c^s (open squares) and $J_{c,1S}^s$ (solid squares), calculated from Eq. (12) and from Eq. (S35) of SM, are the stationary rates of 2S and 1S crystal nucleations; (b) $J_{c,d}^s$ (open diamonds), calculated from Eq. (13), is the stationary nucleation rate of crystals in droplets, $J_{c,d,\infty}^s$ (dotted line) and $J_{c,d,dis}^s$ (solid diamonds), calculated from Eqs. (S37) and (S38) of SM, are the CNT stationary nucleation rates of crystals in infinitely large droplet and in dispersion of droplets; (c) J_d^s (open circles) and $J_{d,1S}^s$ (solid circles), calculated from Eqs. (14) and Eq. (S36) of SM, are the stationary rates of 2S and 1S droplet nucleations. The solid and dashed lines are drawn to guide the eye.

Looking first at the stationary rates J_c^s and $J_{c,1S}^s$ of 2S and 1S ice crystal nucleations in the steam, the open and the solid squares in Fig. 6a, we observe that whereas J_c^s is up to nearly four-fold higher than $J_{c,1S}^s$ for $s_{co} \le 3$ (see the inset in the figure), for $s_{co} > 3$ it is dramatically, up to 13 orders of magnitude, below $J_{c,1S}^s$. Besides, the increase of s_{co} from 4.5 to 5.5 brings about a decrease of J_c^s, and only for $s_{co} > 5.5$ does J_c^s begin again to increase with s_{co}. This is paradoxical from the viewpoint of CNT which, as evidenced by our numerical data for $J_{c,1S}^s$ (the solid squares), predicts a monotonic rise of the 1S crystal nucleation rate with s_{co} in the whole range from 2 to 6. As illustrated in Fig. S3 of SM, the reason for this behavior of J_c^s is in the subtle interplay between the three kinds of cluster fluxes that contribute to the 2S crystal nucleation rate from Eq. (12). Jointly, the stationary flux $K^s \equiv K_{i_{co}*,i_{co}*}^s$ of crystals on the $n = i$ diagonal in the cluster size space and the collective stationary flux $G^s \equiv \sum_{i=i_{co}*+1}^{M-1} G_{i,i-1}^s$ of crystallizing composites supply the diagonal with $i > i_{co}*$-sized crystal supernuclei, but the collective stationary flux $I^s \equiv \sum_{i=i_{co}*+1}^{M-1} I_{i,i}^s$ of crystals that transit into composites by attaching O-phase monomers removes such supernuclei from the diagonal (see Fig. 6a in Ref. [38]). When $s_{co} \le 3$ ($w_{i,n}$ peak practically

inside the triangular cluster size space of 2S nucleation, Figs. 4a and 4b), the positive G^s flux prevails over the positive I^s flux so that the overall $G^s - I^s$ flux is positive and adds to the always positive K^s flux which is a monotonically increasing function of s_{co}. As a result, $J_c^s > J_{c,1S}^s$ for $s_{co} \le 3$ (Fig. 6a). When $s_{co} > 3$, however, the $w_{i,n}$ peak is outside the 2S nucleation cluster-size triangle (Fig. 4c), the overall $G^s - I^s$ flux becomes increasingly more negative because of dominance of I^s over G^s, it subtracts from the K^s flux, and this makes J_c^s drop below $J_{c,1S}^s$ and pass through a maximum at $s_{co} = 4.5$. Nonetheless, for $s_{co} \ge 5.5$, though smaller than $J_{c,1S}^s$, J_c^s is again an increasing function of the supersaturation, because then the increase of the positive K^s flux outpaces the increase in the absolute value of the negative $G^s - I^s$ flux (Fig. S3 of SM). We note and emphasize that, especially for $s_{co} \ge 3.5$, this behavior of J_c^s is influenced by the finite-size effect intrinsic to our results because of our use of $M = 240$ as the maximal cluster size in the numerical solution of Eq. (6) (this effect is considered in SM, see Figs. S4a and S4b therein). Yet, although the $J_c^s(s_{co})$ dependence in Fig. 6a is specific for the attachment/detachment frequencies and the values of the physical parameters used by us in solving Eq. (6), the general conclusion is that $J_c^s < J_{c,1S}^s$ for supersaturations at which the overall stationary $G^s - I^s$ flux is negative. In our case this is so for $s_{co} \ge 3.5$, i.e. in the s_{co} range in which, according to the $i^* < n^*$ criterion [38], the 2S nucleation of ice crystals prevails over their 1S nucleation (see Fig. 4c). This finding is important, because it demonstrates that occurrence of 2S nucleation does not necessarily imply that J_c^s is greater than $J_{c,1S}^s$.

The second to consider is the stationary nucleation rate $J_{c,d}^s$ of ice crystals in the water droplets. It is seen in Fig. 6b that, like $J_{c,1S}^s$, this rate (the open diamonds) is a monotonically increasing function of the supersaturation. For comparison, as illustrated by the solid diamonds in this figure, the stationary rate $J_{c,d,dis}^s$ of crystal nucleation in dispersed $Z_{i,1}^s$ droplets of sufficiently large supernucleus size i also increases monotonically for all supersaturations. The rate $J_{c,d,dis}^s$ is given by Eq. (S38) of SM, and the inset in Fig. 6b shows

that this equation describes the numerically obtained $J^s_{c,d}(s_{co})$ dependence (the open diamonds) with an error of less than one order of magnitude for s_{co} between 2.2 and 5. The dotted line in Fig. 6b represents the s_{co}-independent value of the stationary rate $J^s_{c,d,\infty}$ of homogeneous nucleation of crystals in the bulk M-phase (in our case, a macroscopically large droplet). This value is calculated from Eq. (S37) of SM.

Last, we consider the stationary rates J^s_d and $J^s_{d,1S}$ of 2S and 1S droplet nucleations (whereas in the former process the droplets are involved in 2S crystal nucleation, in the latter process they are not). In Fig. 6c and its inset we see that J^s_d (the open circles) is practically equal to $J^s_{d,1S}$ (the solid circles) for all supersaturations, especially for $s_{co} \le 5$. Thus, in the scope of our model for nucleation work and attachment/detachment frequencies, the effect of 2S nucleation of ice crystals on the homogeneous nucleation of water droplets in steam at $T \approx 220-230$ K is insignificant. As already noted, this is an important indication that the failure of CNT to describe experimental data for the nucleation rate of these droplets in this temperature range [40–43,47] is hardly attributable to undetected formation of ice crystals in the droplets and/or the steam. Both these experimental data and our J^s_d data from Fig. 6c are shown in Fig. S5 of SM, and the issue is further discussed in Section S8 of SM.

Finally, we note that, to check our results for $J^s_{c,1S}$ and $J^s_{d,1S}$ obtained from the numerical solution of Eq. (6), we calculated these rates with the help of the exact Becker-Döring formula [4,39] for stationary 1S nucleation. We found that, as it should be, the $J^s_{c,1S}$ and $J^s_{d,1S}$ values from Eqs. (S35) and (S36) of SM were equal to those from the solution of Eq. (6) for all s_{co}.

4.6. Number density of supernuclei

When the O-phase initially contains no clusters of supernucleus size, the experimentally accessible number density N (m^{-3}) of any kind of supernuclei at time t is obtainable by integration of the respective nucleation rate J, i.e. $N(t) = \int_0^t J(t')dt'$ [4]. Hence, using the nucleation rates from Eqs. (12)–(14) and from Eqs. (S35) and (S36) of SM, we can

determine the number densities N_c and $N_{c,1S}$ of 2S- and 1S-nucleated crystal supernuclei of size $i > i_{co}*$ in the O-phase, the number density $N_{c,d}$ of $n > n*$-sized crystal supernuclei in the composites of size $i \geq n*+1$, and the number densities N_d and $N_{d,1S}$ of $i > i*$-sized supernucleus droplets (which in our case are the M-phase supernuclei) formed, respectively, in the course of 2S crystal nucleation and in the 1S process of droplet nucleation described by CNT. These $N(t)$ dependences are depicted in Fig. 5 for supersaturations $s_{co} = 2.5$, 3 and 5 (left, middle and right column of panels, respectively). In accordance with Eqs. (S41) and (S42) of SM, they are obtained by numerical integration of the $J(t)$ functions in the same figure. Other three $N(t)$ dependences (for composites, for droplets plus composites, and for droplets plus composites plus crystals) are presented in Fig. S1 of SM.

In Fig. 5 we see that for all supersaturations, after a certain delay, all $N(t)$ dependences (the solid and the thick dashed lines) become linear (the thin dashed lines) with slope equal to the stationary nucleation rate represented by dotted line in the corresponding $J(t)$ panel. This is so even for the number density N_c of 2S-nucleated ice crystals in steam at $s_{co} = 5$, which is seen in Fig. 5f to plateau after $t = 0.6$ μs. In fact, however, then N_c is so slightly sloped that it only looks like having a plateau: the slope corresponds to stationary nucleation rate $J_c^s = 3.35 \times 10^{15}$ m^{-3} s^{-1} which, when presented in Fig. 5c, virtually coincides with the zero on the J_c axis. Thus, while a well-manifested asymptotic linearity of $N_c(t)$ allows an easy determination of the stationary rate J_c^s of 2S crystal nucleation when this rate is high enough, a plateau of $N_c(t)$ may well conceal a too low rate J_c^s. In the same fashion, the number density $N_{c,d}$ of crystals in droplets may have an apparent plateau with a low stationary rate $J_{c,d}^s$ hidden by it. Indeed, in Fig. 5j we observe that at $s_{co} = 2.5$ such $N_{c,d}$ plateau would begin at around $t = 10$ μs if the maximum of $J_{c,d}$ in Fig. 5g were much higher. However, as this maximum is not high enough, $N_{c,d}$ in Fig. 5j has only an initial plateau-like disturbance after which it rises linearly, thus making easy the determination of $J_{c,d}^s$.

4.7. Delay time of nucleation

In 1S nucleation, the experimentally accessible delay time θ of the process is defined as the time intercept of the long-time linear portion of the $N(t)$ dependence [4] (see the $N_{c,1S}(t)$ and $N_{d,1S}(t)$ lines in Fig. 5). Physically, θ is a measure of the time needed for attaining stationary nucleation when the supersaturation is kept fixed. Mathematically, it is given by the expression (Eq. (15.99) of Ref. [4]) $\theta = \int_0^\infty [1 - J(t)/J^s]dt$ which, upon recalling that $N(t) = \int_0^t J(t')dt'$, can be represented in the form

$$\theta = \left[t - \frac{N(t)}{J^s} \right]_{t\to\infty} . \tag{15}$$

This equation says that θ is the difference between any time t and the N/J^s ratio at the same t provided t refers to a moment at which nucleation is already stationary (e.g., the final moments of the $N_{c,1S}(t)$ and $N_{d,1S}(t)$ lines in Fig. 5).

Using the same definition of nucleation delay time and the ensuing Eq. (15), again from the linear portions of the different $N(t)$ dependences given by Eqs. (S41) and (S42) of SM (the thin dashed lines in Figs. 5d–5f, 5j–5l and 5p–5r), we can determine θ in 2S nucleation. Now, however, this definition is of limited use, because in some cases Eq. (15) may lead to negative θ values which are an indication for the presence of a sufficiently high initial peak in the respective nonstationary nucleation rate $J(t)$. For example, in Fig. 5f we observe that at $s_{co} = 5$ the long-time increase of N_c with t is so small that, if extrapolated to short times, the linear, almost horizontal portion of N_c would cross the t axis at a negative delay time θ_c of 2S crystal nucleation (see also Fig. 5j in which, similarly, the $N_{c,d}(t)$ dependence has a negative delay time $\theta_{c,d}$). At $s_{co} = 2.5$ and 3, however, the J_c peak is so low (Figs. 5a and 5b) that, as seen in Figs. 5d and 5e, θ_c has positive values and is distinctly longer than the corresponding delay time $\theta_{c,1S}$ of 1S crystal nucleation. Thus, when the initial peak of a nonstationary nucleation rate is absent or is not too high, θ can again be positive (see also Figs. 5m–5r for the droplet nucleation rates and the droplet number densities).

The s_{co} dependences of the various nucleation delay times obtained by means of Eq. (15) (with the end t value of computation considered as infinitely long time) are displayed in Fig. 7. The open and the solid squares in panel (a) represent, respectively, the delay times θ_c

and $\theta_{c,1S}$ in 2S and 1S nucleation of ice crystals in steam, and the diamonds in the same panel refer to the nucleation delay time $\theta_{c,d}$ of ice crystals in droplets. Similarly, panel (b) exhibits the delay time θ_d (open circles) of the nucleation of droplets involved in 2S crystal nucleation and the delay time $\theta_{d,1S}$ (solid circles) of 1S droplet nucleation. Other three $\theta(s_{co})$ dependences (for composites, for droplets plus composites, and for droplets plus composites plus crystals) are presented in Fig. S6 of SM. Numerically, the data for all delay times are given in Table S2 of SM. The table includes the negative values of θ_c for $s_{co} < 2.5$ and $s_{co} > 3.5$ as well as of $\theta_{c,d}$ for $s_{co} < 3$, which cannot be shown on the $\lg\theta$ scale in Fig. 7a. As to the finite-size effect of M on the nucleation delay times, it turns out that in our case it is felt only by θ_c and $\theta_{c,d}$, and Fig. S7 of SM illustrates this.

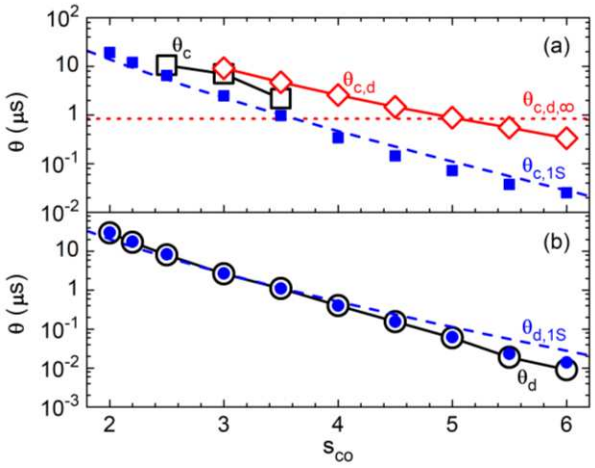

Fig. 7. Supersaturation dependence of nucleation delay time. (a) Open and solid squares – delay times θ_c and $\theta_{c,1S}$ of 2S and 1S crystal nucleation, respectively; diamonds – delay time $\theta_{c,d}$ of nucleation of crystals in droplets. (b) Open and solid circles – delay times θ_d and $\theta_{d,1S}$ of 2S and 1S droplet nucleation, respectively. All data are obtained by means of Eq. (15), the dashed lines graph $\theta_{c,1S}$ and $\theta_{d,1S}$ from Eqs. (S45) and (S46) of SM, the dotted line visualizes the $\theta_{c,d,\infty}$ value from Eq. (S47) of SM, and the solid lines are drawn to guide the eye.

In Fig. 7 we see that all delay times shorten with increasing supersaturation. For s_{co} between 2.5 and 3.5, θ_c is about two to three times greater than $\theta_{c,1S}$. On the other hand, in this s_{co} range, θ_c is up to twice smaller than $\theta_{c,d}$ which, in its turn, is almost up to five-fold greater than $\theta_{c,1S}$ at $s_{co} = 3.5$. When the supersaturation is even higher, $\theta_{c,d}$ remains about one order of magnitude greater than $\theta_{c,1S}$. Thus, θ_c and $\theta_{c,d}$ considerably greater than $\theta_{c,1S}$ for $s_{co} \geq 3$ is an indication for dominant 2S crystal nucleation in this s_{co} range, because it merely reflects the fact that then the droplet nucleation (first step) antecedes the crystal nucleation in the droplets (second step). Regarding the delay times θ_d and $\theta_{d,1S}$ of 2S and 1S droplet nucleation (Fig. 7b), we note that they are practically equal in the entire supersaturation range.

It is of interest to verify whether an approximate, but general CNT expression for the delay time of 1S nucleation [51] is in concordance with the $\theta_{c,1S}(s_{co})$ and $\theta_{d,1S}(s_{co})$ data in Fig. 7. Owing to Eqs. (5.1), (13.36) and (15.105) of Ref. [4], this expression can be represented as $\theta = 4m^*/sf^*$ where s is the dimensionless supersaturation, and f^* is the frequency of monomer attachment to nucleus of size m^*. As shown in Section S10 of SM, this leads to Eqs. (S45) and (S46) for the dependences of $\theta_{c,1S}$ and $\theta_{d,1S}$ on s_{co} which are illustrated in Fig. 7 by dashed lines (as indicated). We see that they describe fairly well the numerical data (solid squares and circles) over the whole s_{co} range in which $\theta_{c,1S}$ and $\theta_{d,1S}$ change about three orders of magnitude.

Likewise, it is of interest to see how different the delay time $\theta_{c,d}$ of crystal nucleation in the droplets is from the CNT s_{co}-independent delay time $\theta_{c,d,\infty}$ of nucleation of the crystals in bulk M-phase (macroscopically large droplet). In this case, the above general expression for θ leads to Eq. (S47) of SM, which yields $\theta_{c,d,\infty} = 0.84$ μs. This $\theta_{c,d,\infty}$ value is visualized by the dotted line in Fig. 7a. We observe that the s_{co}-independent $\theta_{c,d,\infty}$ provides only a tentative estimate of $\theta_{c,d}$ which diminishes with s_{co} from 9.1 to 0.34 μs for s_{co} from 3 to 6.

5. Conclusion

The composite-cluster model with cluster formation work $w_{i,n}$ from Eq. (5) and monomer attachment frequencies $f_{i,n}$, $g_{i,n}$ and $k_{i,i}$ from Eqs. (S10)–(S12) of SM is perhaps the simplest possible model of 2S crystal nucleation. Notwithstanding the simplicity of this CNT-inspired model, the present study provides unprecedented mechanistic insight into the peculiarities of the kinetics of 2S crystal nucleation. Among the results obtained, several seem most important and deserve bringing to the fore.

Together with Eqs. (2) and (3), the master equation of 2S nucleation, Eq. (1), is a solid basis for analyzing the kinetics of this highly complicated process. With appropriate, sufficiently elaborate models for $w_{i,n}$, $f_{i,n}$, $g_{i,n}$ and $k_{i,i}$, this equation can be used for determination of the crystal, composite, and droplet size distributions and nucleation rates in a wealth of cases of both academic and technological interest.

In the scope of the composite-cluster model with $w_{i,n}$ from Eq. (5) and $f_{i,n}$, $g_{i,n}$ and $k_{i,i}$ from Eqs. (S10)–(S12) of SM, in homogeneous 2S ice crystal nucleation in steam below the water freezing temperature, the stationary cluster size distributions of the water droplets and the ice crystals in the steam resemble those in homogeneous 1S nucleation of the droplets and the crystals. Among the water composites with the size i^* of the droplet nucleus those with n^*-sized ice crystal nucleus in them are the least populated species.

Again in the scope of the same model, at both low ($s_{co} < 2.5$) and high ($s_{co} > 3.5$) supersaturations, the nonstationary 2S nucleation rate J_c of ice crystals in the steam has a high initial peak after which it plateaus at a stationary value J_c^s which can be much smaller than the value $J_{c,1S}^s$ of the stationary 1S nucleation rate of the crystals. At intermediate supersaturations, J_c is a distorted sigmoidal function of time, more or less different from the strictly sigmoidal nonstationary 1S crystal nucleation rate. High initial peak also characterizes the nonstationary rate $J_{c,d}$ of ice crystals in the water droplets, but only when $s_{co} < 3$; this rate is virtually perfectly sigmoidal at higher supersaturations. The nonstationary nucleation rate J_d of the water droplets is practically indistinguishable from the CNT-predicted, sigmoidally-shaped nonstationary rate $J_{d,1S}$ of 1S droplet nucleation.

Perhaps surprisingly, our study demonstrates that the stationary 2S crystal nucleation rate J_c^s is not necessarily higher than the corresponding stationary rate $J_{c,1S}^s$ of 1S crystal nucleation. In our case, $J_c^s << J_{c,1S}^s$ when the supersaturation is so high ($s_{co} > 3$) that the 2S

nucleation of the ice crystals prevails over their 1S nucleation, because then $i^* < n^*$. The stationary nucleation rate J_d^s of the water droplets is practically unaffected by the 2S nucleation of the ice crystals, which is an indication that the well-known failure of CNT to describe experimental data for water droplet nucleation in steam below the water freezing temperature is quite likely not caused by undetected nucleation of ice crystals in the droplets and the steam.

Whereas the delay time θ_c of 2S crystal nucleation is negative for $s_{co} < 2.5$ and $s_{co} > 3.5$, the delay time $\theta_{c,d}$ of crystal nucleation in the droplets is negative only for $s_{co} < 3$. The reason is the presence of a sufficiently high initial peak in the J_c time dependence for these low and high supersaturations and in the $J_{c,d}$ time dependence for these low supersaturations. When J_c and $J_{c,d}$ are nearly sigmoidally shaped functions of time and, accordingly, θ_c and $\theta_{c,d}$ are positive, both $\ln \theta_c$ and $\ln \theta_{c,d}$ diminish almost linearly with s_{co}.

Declaration of competing interest

The authors declare that they have no known competing financial interests or personal relationships that could have appeared to influence the work reported in this paper.

Acknowledgement

Fruitful discussions of one of the authors (D. K.) with Prof. Bogdan Ranguelov are gratefully acknowledged.

Appendix A. Supplementary material

Supplementary data associated with this article can be found, in the online version, at https://doi.org/

References

[1] M. Volmer, A. Weber, Z. Phys. Chem. 119 (1926) 277.

[2] M. Volmer, Kinetik der Phasenbildung, Steinkopff, Dresden, 1939.

[3] A.E. Nielsen, Kinetics of Precipitation, Pergamon, Oxford, 1964.

[4] D. Kashchiev, Nucleation: Basic Theory with Applications, Butterworth-Heinemann, Oxford, 2000.

[5] P.R. ten Wolde, D. Frenkel, Science 277 (1997) 1975.

[6] P.G. Vekilov, Cryst. Growth Des 4 (2004) 671.

[7] T.H. Zhang, X.Y. Liu, J. Phys. Chem. B 111 (2007) 14001.

[8] C. Degranges, J. Delhommelle, Phys. Rev. Lett. 98 (2007) 235502.

[9] L.B. Gower, Chem. Rev. 108 (2008) 4551.

[10] J.A. van Meel, A.J. Page, R.P. Sear, D. Frenkel, J. Chem. Phys. 129 (2008) 204505.

[11] E.M. Pouget, P.H.H. Bomans, J.A.C.M. Goos, P.M. Frederik, G. de With, N.A.J.M. Sommerdijk, Science 323 (2009) 1455.

[12] J.R. Savage, A.D. Dinsmore, Phys. Rev. Lett. 102 (2009) 198302.

[13] N. Duff, B. Peters, J. Chem. Phys. 131 (2009) 184101.

[14] P.G. Vekilov, Cryst. Growth Des. 10 (2010) 5007.

[15] D. Gebauer, H. Cölfen, Nano Today, 6 (2011) 564.

[16] J.R. Savage, L. Pei, A.D. Dinsmore, Adv. Chem. Phys. 151 (2012) 111.

[17] M. Salvalaglio, C. Perego, F. Giberti, M. Mazzotti, M. Parrinello, Proc. Natl. Acad. Sci. USA 112 (2015) E6.

[18] W. Qi, Y. Peng, Y. Han, R.K. Bowles, M. Dijkstra, Phys. Rev. Lett. 115 (2015) 185701.

[19] A. Sauter, F. Roosen-Runge, F. Zhang, G. Lotze, R.M.J. Jacobs, F. Schreiber, J. Am. Chem. Soc. 137 (2015) 1485.

[20] S. Karthika, T.K. Radhakrishnan, P. Kalaichelvi, Cryst. Growth Des. 16 (2016) 6663.

[21] G.C. Sosso, J. Chen, S.J. Cox, M. Fitzner, P. Pedevilla, A. Zen, A. Michaelides, Chem. Rev. 116 (2016) 7078.

[22] Y. Bi, A. Porras, T. Li, J. Chem. Phys. 145 (2016) 211909.

[23] P.G. Vekilov, Prog. Cryst. Growth Charact. Mater. 62 (2016) 136.

[24] P.J.M. Smeets, A.R. Finney, W.J.E.M. Habraken, F. Nudelman, H. Friedrich, J. Laven, J.J. De Yoreo, P.M. Rodger, N.A.J.M. Sommerdijk, Proc. Natl. Acad. Sci. USA 114 (2017) E7882.

[25] T.H. Zhang, Z.C. Zhang, J.S. Cao, X.Y. Liu, Phys. Chem. Chem. Phys. 21 (2019) 7398.

[26] D. James, S. Beairsto, C. Hartt, O. Zavalov, I. Saika-Voivod, R.K. Bowles, P.H. Poole, J. Chem. Phys. 150 (2019) 074501.

[27] J. Shao, Y. Yang, P. Tang, Polymers 210 (2020) 122960.

[28] T. Nakamuro, M. Sakakibara, H. Nada, K. Harano, E. Nakamura, J. Am. Chem. Soc. 143 (2021) 1763.

[29] P.E. L'vov, A.R. Umantsev, Cryst. Growth Des. 21 (2021) 366.

[30] V. Leffler, S. Ehlert, B. Förster, M. Dulle, S. Förster, ACS Nano 15 (2021) 840.

[31] S. Xu, H. Zhang, B. Qiao, Y. Wang, Cryst. Growth Des. 21 (2021), https://doi: 10.1021/acs.cgd.0c01376.

[32] R.K.R. Addula, S.N. Punnathanam, Phys. Rev. Lett. 126 (2021) 146001.

[33] D. Eaton, I. Saika-Voivod, R.K. Bowles, P.H. Poole, J. Chem. Phys. 154 (2021) 234507.

[34] K. Z. Takahashi, T. Aoyagi, J.-i. Fukuda, Nat. Commun. 12 (2021) 5278.

[35] M. Iwamatsu, J. Chem. Phys. 134 (2011) 164508.

[36] M. Iwamatsu, J. Chem. Phys. 136 (2012) 204702.

[37] M. Iwamatsu, Phys. Rev. E 86 (2012) 041604.

[38] D. Kashchiev, J. Cryst. Growth 530 (2020) 125300.

[39] R. Becker, W. Döring, Ann. Phys. (Leipzig) 24 (1935) 719.

[40] R.C. Miller, R.J. Anderson, J.L. Kassner, Jr., D.E. Hagen, J. Chem. Phys. 78 (1983) 3204.

[41] J. Wölk, R. Strey, J. Phys. Chem. B 105 (2001) 11683.

[42] Y.J. Kim, B.E. Wyslouzil, G. Wilemski, J. Wölk, R. Strey, J. Phys. Chem. A 108 (2004) 4365.

[43] V. Holten, D.G. Labetski, M.E.H. van Dongen, J. Chem. Phys. 123 (2005) 104505.

[44] M.M. Campagna, J. Hrubý, M.E.H. van Dongen, D.M.J. Smeulders, J. Chem. Phys. *153*, (2020) 164303.

[45] Y. Tahri, E. Gagnière, E. Chabanon, T. Bounahmidi, Z. Kožišek, N. Candoni, S. Veesler, M. Boukerche, D. Mangin, Cryst. Growth Des. 19 (2019) 3329.

[46] D. Kashchiev, K. Sato, J. Chem. Phys. 109 (1998) 8530.

[47] D. Kashchiev, J. Chem. Phys. 125 (2006) 044505.

[48] K. Ahnert, M. Mulansky, AIP Conf. Proc. 1389 (2011) 1586.

[49] A. Devert, Matplotlib Plotting Cookbook, Packt, Birmingham, 2014.

[50] D. Kashchiev, P.G. Vekilov, A.B. Kolomeisky, J. Chem. Phys. 122 (2005) 244706.

[51] D. Kashchiev, Surface Sci. 14 (1969) 209.

Figure captions

(single-column fitting)
Fig. 1 (color online only). (a) Schematic of composite cluster of i monomers with n-sized M-phase cluster in it (top), of crystal cluster of i monomers (bottom left) in O-phase, and of M-phase cluster of i monomers (bottom right) (the arrows illustrate the frequencies $f_{i,n}$, $g_{i,n}$, $f_{i,i}$, $k_{i,i}$ and $f_{i,1}$ of monomer attachment to the respective clusters). (b) The triangular i,n cluster-size space with the $I_{i,n}$, $G_{i,n}$, and $K_{i,i}$ fluxes (shown by arrows) that control the nucleation and growth of M-phase and composite clusters, of crystals in the M-phase, and of crystals in the O-phase, respectively. The $I_{i,i}$ arrow visualizes the flux of i,i-sized crystals in the O-phase that transit to $i+1,i$-sized composites, and the circles represent points i,n and i,i in the size space.

(single-column fitting)
Fig. 2 (color online only). Contour plot (the borderlines between the ellipsoidal strips) of the cluster formation work $w_{i,n}$ from Eq. (5) with superimposed front of the cluster concentration $Z_{i,n}$ from Eq. (8) at successive times (indicated in μs) of 2S nucleation when (a) $s_{co}=2.5$ (then $i^*>n^*$), (b) $s_{co}=3$ (then $i^*\approx n^*$), and (c) $s_{co}=5$ (then $i^*<n^*$). The concentration of i,n-sized clusters on a front line at any time t is $Z_{i,n}(t)=1$ km^{-3} in panel (a), 1 m^{-3} in panel (b) and 1 mm^{-3} in panel (c). In each panel, the star visualizes the position i^*,n^* of the $w_{i,n}$ maximum, the square on the $n=i$ line indicates the size i_{co}^* of the ice crystal nucleus in the steam, and the vertical and horizontal lines represent the i^* and n^* ridges of the $w_{i,n}$ surface, respectively. The $w_{i,n}$ scale is on the right of the panels.

(two-column fitting)
Fig. 3 (color online only). Cluster size distributions from Eq. (8) at $s_{co}=2.5$ (left column of panels), $s_{co}=3$ (middle column of panels), and $s_{co}=5$ (right column of panels). $Z_{i,i}$, $Z_{i,1}$, Z_{i,n^*}, and $Z_{i^*,n}$ refer, respectively, to ice crystals in steam, water droplets, water composites containing the n^*-sized ice crystal nucleus, and ice crystals within those composites that are with the size i^* of the droplet nucleus. The numbers at the lines indicate the time (in μs) elapsed from the onset of the 2S nucleation process. The dashed lines represent the corresponding equilibrium cluster size distributions $C_{i,i}$, $C_{i,1}$, C_{i,n^*}, and $C_{i^*,n}$ from Eq. (4).

(single-column fitting)
Fig. 4 (color online only). Cluster flow lines dictated by the fluxes from Eqs. (9)–(11) in stationary 2S nucleation when: (a) $s_{co}=2.5$, (b) $s_{co}=3$, and (c) $s_{co}=5$ (then $i^*>n^*$, $i^*\approx n^*$, and $i^*<n^*$, respectively). The arrow heads indicate the flow direction, and the background is the $w_{i,n}$ contour plot from Fig. 2. In each panel, the star visualizes the position i^*,n^* of the $w_{i,n}$ maximum, the square on the $n=i$ line indicates the size i_{co}^* of the ice crystal nucleus in the steam, the vertical and horizontal lines represent the i^* and n^* ridges of the $w_{i,n}$ surface, respectively, and the upper triangular part of the contour plot is obscure, because it is in the physically inaccessible i,n cluster size space. The $w_{i,n}$ scale is on the right of the panels.

(two-column fitting)
Fig. 5 (color online only). Time dependence of the nucleation rates J and the number densities N of supernuclei from Eqs. (12)–(14) and from Eqs. (S35), (S36), (S41) and (S42) of SM at $s_{co} = 2.5$ (left column of panels), $s_{co} = 3$ (middle column of panels), and $s_{co} = 5$ (right column of panels). The dotted lines in the $J(t)$ panels represent the respective stationary nucleation rates, the thin dashed lines in the $N(t)$ panels are the long-time $N(t)$ asymptotes, and the arrows in these panels indicate the respective delay times of nucleation.

(single-column fitting)
Fig. 6 (color online only). Supersaturation dependence of stationary nucleation rate: (a) J_c^s (open squares) and $J_{c,1S}^s$ (solid squares), calculated from Eq. (12) and from Eq. (S35) of SM, are the stationary rates of 2S and 1S crystal nucleations; (b) $J_{c,d}^s$ (open diamonds), calculated from Eq. (13), is the stationary nucleation rate of crystals in droplets, $J_{c,d,\infty}^s$ (dotted line) and $J_{c,d,dis}^s$ (solid diamonds), calculated from Eqs. (S37) and (S38) of SM, are the CNT stationary nucleation rates of crystals in infinitely large droplet and in dispersion of droplets; (c) J_d^s (open circles) and $J_{d,1S}^s$ (solid circles), calculated from Eqs. (14) and Eq. (S36) of SM, are the stationary rates of 2S and 1S droplet nucleations. The solid and dashed lines are drawn to guide the eye.

(single-column fitting)
Fig. 7 (color online only). Supersaturation dependence of nucleation delay time. (a) Open and solid squares – delay times θ_c and $\theta_{c,1S}$ of 2S and 1S crystal nucleation, respectively; diamonds – delay time $\theta_{c,d}$ of nucleation of crystals in droplets. (b) Open and solid circles – delay times θ_d and $\theta_{d,1S}$ of 2S and 1S droplet nucleation, respectively. All data are obtained by means of Eq. (15), the dashed lines graph $\theta_{c,1S}$ and $\theta_{d,1S}$ from Eqs. (S45) and (S46) of SM, the dotted line visualizes the $\theta_{c,d,\infty}$ value from Eq. (S47) of SM, and the solid lines are drawn to guide the eye.